

Article

Fluorescence vs. Phosphorescence: Which Scenario Is Preferable in Au(I) Complexes with Benzothiadiazoles?

Radmir. M. Khisamov, Alexey A. Ryadun, Sergey N. Konchenko and Taisiya S. Sukhikh * 

Nikolaev Institute of Inorganic Chemistry, Siberian Branch of the Russian Academy of Sciences, 3 Lavrentiev Ave., 630090 Novosibirsk, Russia

* Correspondence: sukhikh@niic.nsc.ru

Abstract: The photoluminescence of Au(I) complexes is generally characterized by long radiative lifetimes owing to the large spin-orbital coupling constant of the Au(I) ion. Herein, we report three brightly emissive Au(I) coordination compounds, **1**, **2a**, and **2b**, that reveal unexpectedly short emission lifetimes of 10–20 ns. Polymorphs **2a** and **2b** exclusively exhibit fluorescence, which is quite rare for Au(I) compounds, while compound **1** reveals fluorescence as the major radiative pathway, and a minor contribution of a microsecond-scale component. The fluorescent behaviour for **1–2** is rationalized by means of quantum chemical (TD)-DFT calculations, which reveal the following: (1) S_0-S_1 and S_0-T_1 transitions mainly exhibit an intraligand nature. (2) The calculated spin-orbital coupling (SOC) between the states is small, which is a consequence of overall small metal contribution to the frontier orbitals. (3) The T_1 state features much lower energy than the S_1 state (by ca. 7000 cm^{-1}), which hinders the SOC between the states. Thus, the S_1 state decays in the form of fluorescence, rather than couples with T_1 . In the specific case of complex **1**, the potential energy surfaces for the S_1 and T_2 states intersect, while the vibrationally resolved S_1-S_0 and T_2-S_0 calculated radiative transitions show substantial overlap. Thus, the microsecond-scale component for complex **1** can stem from the coupling between the S_1 and T_2 states.

Keywords: luminescence; Au(I) complexes; TD-DFT calculations; triplet state; single crystal X-ray diffraction; benzothiadiazole



Citation: Khisamov, R.M.; Ryadun, A.A.; Konchenko, S.N.; Sukhikh, T.S. Fluorescence vs. Phosphorescence: Which Scenario Is Preferable in Au(I) Complexes with Benzothiadiazoles? *Molecules* **2022**, *27*, 8162. <https://doi.org/10.3390/molecules27238162>

Academic Editors: Andreas Winter, Ulrich S. Schubert and Benjamin Dietzek-Ivanšić

Received: 7 November 2022

Accepted: 21 November 2022

Published: 23 November 2022

Publisher's Note: MDPI stays neutral with regard to jurisdictional claims in published maps and institutional affiliations.



Copyright: © 2022 by the authors. Licensee MDPI, Basel, Switzerland. This article is an open access article distributed under the terms and conditions of the Creative Commons Attribution (CC BY) license (<https://creativecommons.org/licenses/by/4.0/>).

1. Introduction

Au(I) is a heavy d^{10} ion, whose coordination compounds have widespread applications, particularly in areas associated with light emission [1–4]. For these applications, understanding the origin of photophysical processes and the structure–property relationships is essential, as they play a decisive role in the characteristics of functional materials [5–7]. Au coordination compounds generally reveal a phosphorescent nature of luminescence (both conventional phosphorescence and delayed fluorescence) [8–11], which is tailored by the heavy atom effect. The latter promotes spin-orbit coupling (SOC) between singlet and triplet states, thus facilitating intersystem crossing (ISC) between them, which relaxes the spin ‘forbidden’ radiative transitions [12]. In general, the heavier the metal atom of a coordination compound, the stronger the SOC [13–15]. However, recent studies revealed that the presence of heavy atoms does not guarantee efficient ISC, while the nature of ligands may play a critical role in determining the radiation pathway [16–18]. To this end, the theoretical understanding of the relaxation processes is crucial, especially since conventional ISC between the S_1 and T_1 states is not necessarily the only pathway [19,20]. For instance, in a recently reported Au(III) complex, the S_1 state couples with T_4 and T_5 , resulting in phosphorescence as a major radiation pathway, while the relative Au(I) complex mainly demonstrates fluorescence due to the absence of triplet states energetically close to S_1 [21]. The study of two Pt(II) complexes revealed the existence of two channels, S_1-T_1 and S_1-T_2 ; structural differences in the complexes result in a dominance of either one or the

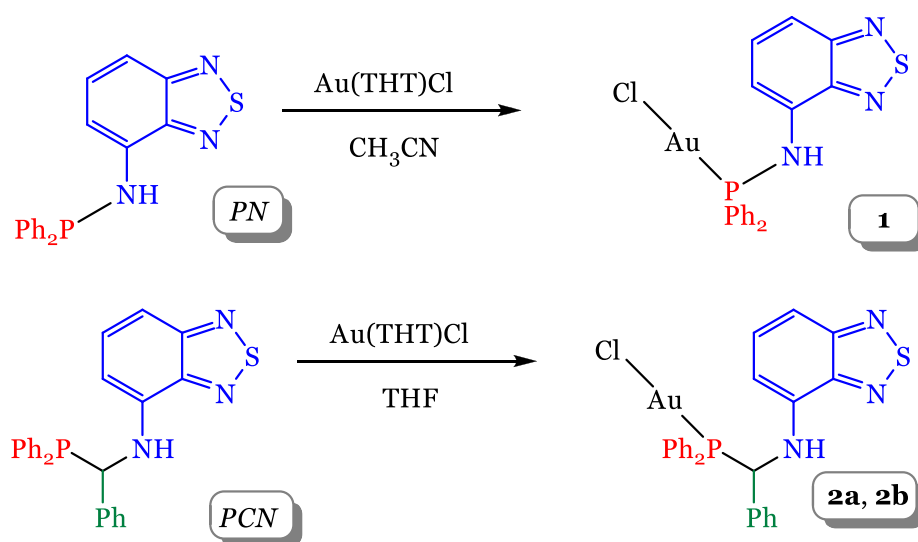
other channel, which induces their different luminescent behaviour [22]. Recently reported benzothiadiazole-based Au(I) compounds feature high quantum yields, reaching 97% in various organic matrices [23]. Notably, in the latter complexes, only a prompt fluorescence was observed.

Inspired by these encouraging examples, we study the luminescent properties of novel Au(I) complexes **1**, **2a**, and **2b** with two closely related ligands bearing benzothiadiazole (btd) moiety. In this context, amino-substituted btds open up a great scope for the design of photoactive materials: a slight variation of the composition and structure of btds results in a wide variation of energetic characteristics of electronic transitions, which is the key to fine-tuning the photophysical properties [24–27]. Herein, we chose two phosphorus-nitrogen ligands, comprising the NH-btd moiety as a chromophore, and PPh₂ moiety as a readily accessible unit for the metal coordination. Synthesized compounds **1–2** exhibit prompt fluorescence, unusual for Au(I) complexes. We provide an interpretation of this phenomenon using quantum chemical DFT calculations.

2. Results and Discussion

2.1. Synthesis and Crystal Structure of the Compounds

The new compound *N*-(diphenylphosphino)-2,1,3-benzothiadiazole-4-amine (PN; Scheme 1) was prepared by the reaction of 4-amino-2,1,3-benzothiadiazole and chlorodiphenylphosphine, in the presence of triethylamine as a base. The corresponding 1,3-phosphinoamine, PCN, was prepared by the one-pot condensation of diphenylphosphine, benzaldehyde, and 4-amino-2,1,3-benzothiadiazole as reported recently [28]. Reactions of equimolar amounts of (THT)AuCl (THT = tetrahydrothiophene) with PN and PCN yielded complexes [Au(PN)Cl] (**1**) and [Au(PCN)Cl] (**2**), respectively. Changing the molar ratio of the phosphinoamines and Au to 1:2 produced the same complexes. For complex **2**, we obtained two polymorphs, **2a** and **2b**. The first one (**2a**) precipitated by slow concentration of a tetrahydrofuran (THF) solution under vacuum, while the second polymorph (**2b**) was formed from oversaturated oily THF solution. Both polymorphs can be obtained as a single phase, as evidenced by powder X-ray diffraction (XRD) analysis (Figures S1–S3).



Scheme 1. Synthesis of compounds **1**, **2a**, and **2b**.

According to single-crystal XRD analysis, compounds **1**, **2a**, and **2b** exhibit a linear coordination environment of the metal by the Cl and P atoms (Figure 1). Except for these, Au(I) reveals neither intra- nor intermolecular contacts. No other specific intermolecular interactions were found. The geometry of molecule **2a** mainly differs from **2b** in the torsion angle {Au–P–C–N} (56.2° in **2a** versus 165.7° in **2b**). According to DFT calculations, the single molecules have similar Gibbs energy (the energy difference is less than 1 kJ·mol^{−1}),

while the calculated energy barrier (both in vacuum and in THF), corresponding to the transition from **2a** to **2b**, amounts to $30 \text{ kJ}\cdot\text{mol}^{-1}$ (Figure 2). This implies that the conformers **2a** and **2b** can easily transform to each other in the solution, which is corroborated by the presence of one set of signals in the corresponding ^{31}P and ^1H NMR spectra. Upon crystallization, either one or the other conformer is implemented, depending on a slight variation in the conditions; specifically, almost the entire amount of the dissolved complex can precipitate as pure phase **2a**.

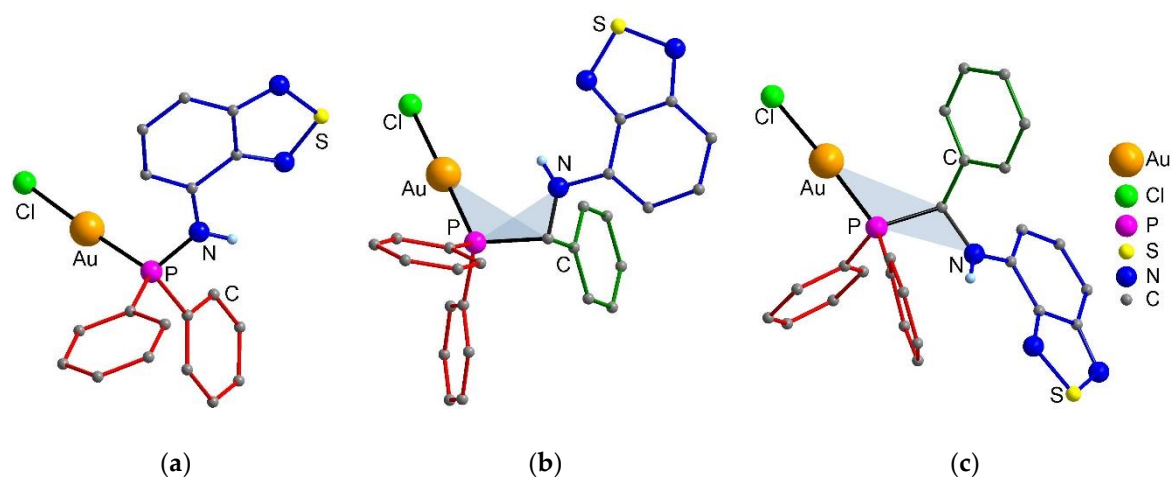


Figure 1. Crystal structures of compounds **1** (a), **2a**, (b) and **2b**, (c). Hydrogen atoms, except those belonging to the NH groups, are omitted. {Au-P-C-N} torsion angles are highlighted with transparent blue triangles.

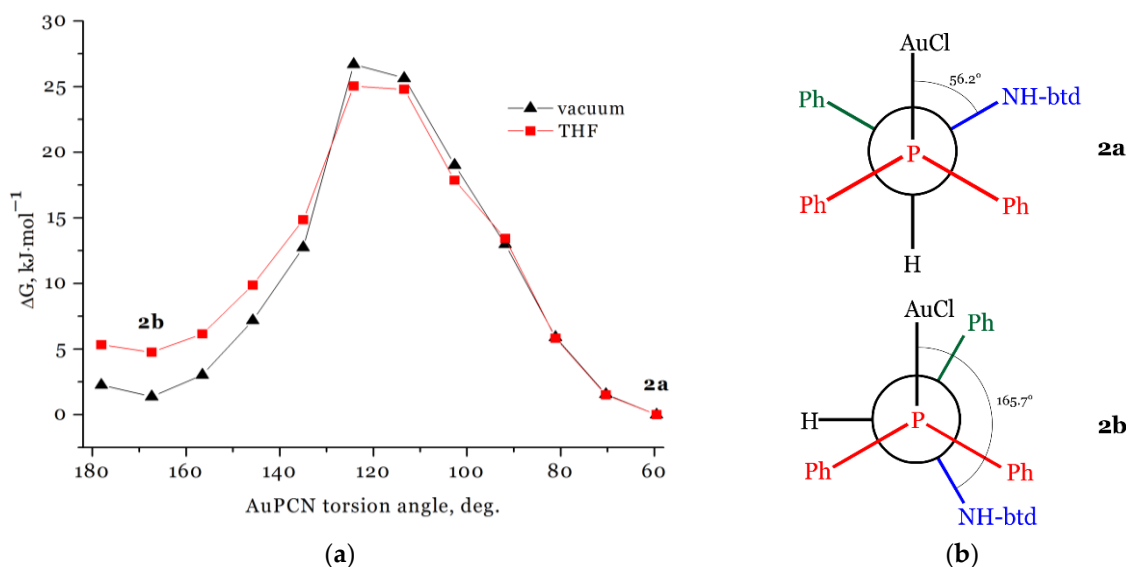


Figure 2. (a) Gibbs energy scans of {AuPPh₂Cl} moiety rotation around the P-C bond for the molecule [Au(PCN)Cl]. (b) Schematic representation of the corresponding conformers **2a** and **2b**.

2.2. Photophysical Properties and TD-DFT Calculations

The UV-Vis spectra were measured for **1–2** in the solid state (Figure 3, Table 1). The shape of the spectra is quite similar, with the exception that the long wavelength band for compound **1** is hypsochromically shifted as compared to **2a** and **2b**. According to TD-DFT calculations for the single molecules at their ground-state optimised geometry (Tables S1–S6), the long wavelength band corresponds to the S_0 – S_1 transition between HOMO and LUMO orbitals (Figure 4, Figures S4 and S5). The transition has a locally excited

(LE) character with a notable contribution of an intraligand charge transfer (ILCT) from the periphery to the thiadiazole moiety, which is common for btd derivatives (Figure 4) [28–31]. In addition, compound **1** features a minor contribution of Au and Cl orbitals to the HOMO, which implies the presence of (M+X)LCT (metal- and halogen-to-ligand charge transfer). Upon photoexcitation, solids **1–2** exhibit a bright emission, with the absolute quantum yields of 30–34% (Table 1). The position of the bands does not depend on the excitation wavelength in the range of 300–400 nm (Figure S6). The luminescence spectra of compounds **2a** and **2b** reveal a hypsochromic shift of the emission band by ca. 450 and 100 cm^{-1} , respectively, compared with free PCN. Compound **1** exhibits a more pronounced hypsochromic shift by ca. 2750 cm^{-1} compared with PN. The absorption and emission spectra of **2a** and **2b** in THF solution (Figure S7) are identical, suggesting that there is one emitting species in the solution.

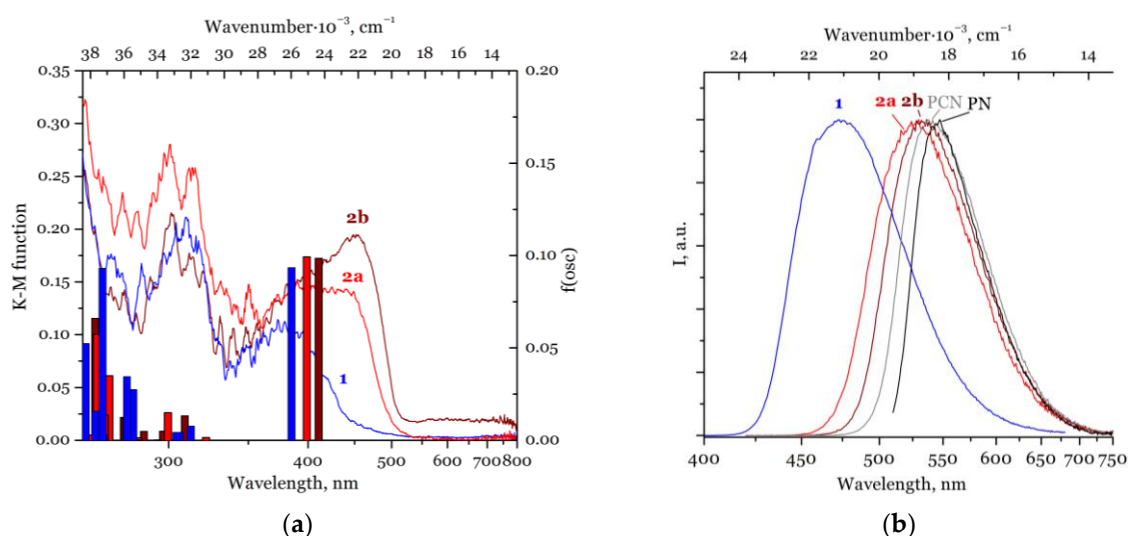


Figure 3. (a) Experimental UV-Vis spectra of solid samples **1–2** mixed with BaSO₄ in the form of Kubelka-Munk functions (lines) and the calculated vertical S_0 – S_n transitions and their oscillator strength (TD-PBE0/def2-TZVP(-f)) (vertical bars). (b) The corresponding experimental normalized photoluminescence spectra (excitation wavelength 350 nm for **1** and 400 nm for **2a** and **2b**).

Table 1. Experimental absorption and emission maxima (λ_{Abs} and λ_{Em}), calculated energies of vertical ($S_0 \rightarrow S_1$) and emission ($S_1 \rightarrow S_0$, $T_1 \rightarrow S_0$ and $T_2 \rightarrow S_0$) transitions (TD(A)-PBE0/def2-TZVP(-f)), experimental emission lifetimes (τ), and absolute quantum yield of the emission (QY; at the excitation by 350 nm) for the compounds.

Compound	λ_{Abs} , nm	$E(S_0 \rightarrow S_1)$, nm	λ_{Em} , nm	$E(S_1 \rightarrow S_0)$, nm	$E(T_1 \rightarrow S_0)$, nm	$E(T_2 \rightarrow S_0)$, nm	τ , μs	τ , ns	QY, %
1	310, 380	384	470	492	798	407	100	10	34
2a	310, 360–500 (br.)	399	525	504	785	404	–	15	30
2b	310, 360–500 (br.)	410	535	512	833	403	–	9, 19	33

Unexpectedly, the emission decay curves of solids **1–2** exhibit kinetics on the nanosecond scale, which yields the emission lifetimes of 10–20 ns (Figures S8–S10). This is not typical for Au complexes, which usually reveal microsecond-scale kinetics owing to efficient SOC between the singlet and triplet states. The emission bands change negligibly upon cooling from room temperature to 77 K (Figure S11). Compounds **2a** and **2b** show exclusively prompt luminescence, while **1** features a weak afterglow signal after a time delay of 300 μs ; the position of the corresponding band approximately coincides with that in the steady-state spectrum (Figure 5a). Thus, we can speculate that both prompt and delayed emission result from the same excited state. Since the microsecond-scale component (with an estimated lifetime of 100 μs) is not detected against the background

of the nanosecond-scale kinetics, we assume it has a contribution of less than 1% of the overall emission.

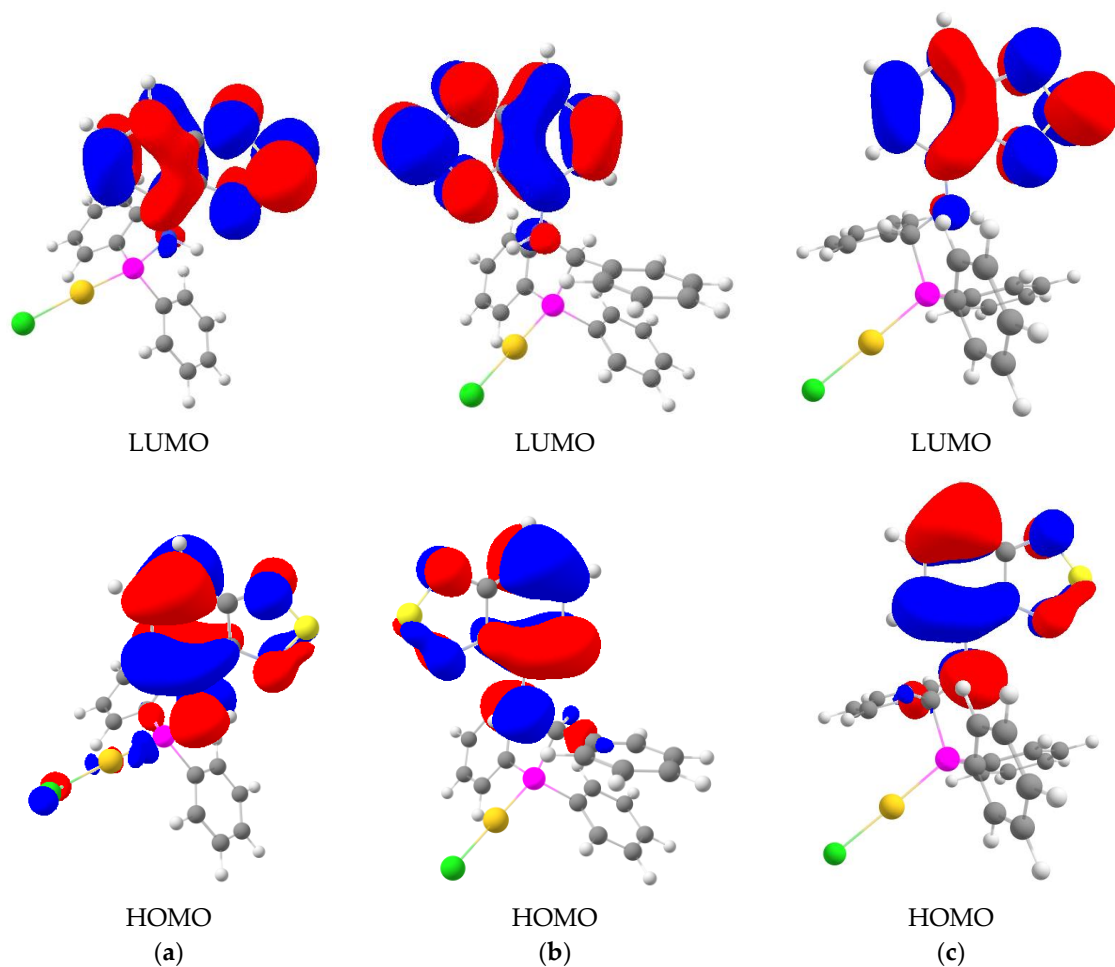


Figure 4. Frontier orbitals for compounds **1** (a), **2a** (b), and **2b** (c) at their S_0 equilibrium geometries (isovalue = 0.03).

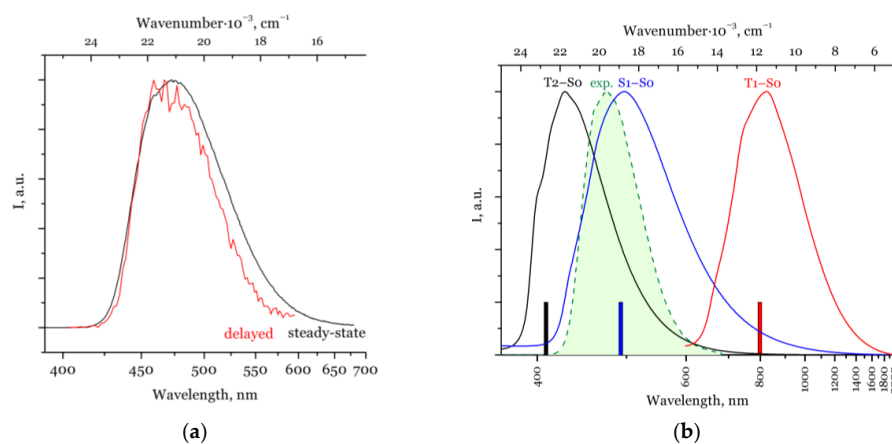


Figure 5. (a) Experimental normalized steady-state and delayed (after 300 μ s) emission spectra of solid sample **1** (excitation wavelength 350 nm). (b) Experimental steady-state emission spectrum of **1** (dashed line) and the corresponding calculated vibrational resolved emission spectra (solid lines) for the transitions from the triplet (T_1 and T_2) and singlet (S_1) states. Vertical bars indicate the corresponding TD-DFT-computed emission energies of the transitions.

One should note that the afterglow intensity decreases under constant irradiation of a sample of **1**, even in deaerated conditions. Within an hour, the signal drops by 10 times under a 450 W source of white light. Under the same conditions, the overall steady-state emission spectrum changes negligibly. This implies that the triplet states decompose due to processes in the solid, and are less photostable compared to the singlet excited states. The afterglow signal and its behaviour persist for samples from several parallel syntheses.

To gain insights into the peculiar fluorescent behaviour of compounds **1–2**, we performed TD-DFT calculations for the emission transitions from the singlet and triplet excited states (Table 1), as well as the SOC matrix elements between these states (Tables S7 and S8). For complexes **2a** and **2b**, the calculated SOC is weak (the coefficients are 10 cm^{-1} and less), which is in line with the observed absence of a phosphorescence. The calculated SOC for **1** is several times higher, which is still quite weak, but it enables the mixing of the singlet and triplet states. For the complexes, the brightest excitation transition in the long wavelength region is S_0-S_1 , while the others (including S_2 and S_3) feature a much shorter wavelength and a 10 times lower magnitude of oscillator strength (Table 2). Therefore, we consider the S_1-T_n channels as the most probable pathways. The calculated T_1 energy level is widely separated from the S_1 level (the difference between vertical S_0-S_1 and S_0-T_1 transitions of ca. 7000 cm^{-1}). This results in a very slow ISC from the S_1 state and thus enables fluorescence from this state. A similar observation was observed for Pt complexes that also feature high $\Delta E(S_1-T_1)$ of 6000 cm^{-1} resulting in the fluorescence along with conventional phosphorescence [32].

Table 2. Calculated characteristics for vertical S_0-S_n ($n = 1-3$) transitions for compounds **1–2**.

n	1			2a			2b		
	λ , nm	f	Electronic States *	λ , nm	f	Electronic States *	λ , nm	f	Electronic States *
1	384	0.093	H→L	399	0.099	H→L	410	0.093	H→L
2	312	0.008	H→L + 1	322	0.002	H→L + 1	309	0.013	H→L + 1
3	306	0.004	H-1→L	300	0.015	H→L + 2	297	0.005	H→L + 2

*—the contribution of all listed orbital transitions is more than 0.97.

For complex **1**, the T_2 level locates energetically much closer to S_1 than does T_1 . Vibrationally resolved calculated T_2-S_0 and S_1-S_0 emission spectra strongly overlap owing to the presence of a large number of vibrational sublevels of the S_1 and T_2 manifolds (Figure 5b). The comparison of energies at different geometry states (Figure 6) revealed that the potential energy surface (PES) for the S_0 state has a local minimum at the T_2 equilibrium geometry, while no imaginary frequencies were found for this geometry. As evidenced by the energy diagram, the PESs for the S_1 and T_2 states intersect: for the equilibrium T_2 -geometry, the energies for the S_1 and T_2 states show reverse order as compared to the equilibrium of the S_1 geometry. Note also that the HOMO orbital for the relaxed T_2 state differs from that for S_1 state by a higher contribution of Au and Cl atoms (Figure S12). In addition, the SOC matrix elements between S_1 and T_2 at the T_2 equilibrium geometry are almost twice as large as those at the S_0 and S_1 geometries (Table S8). Therefore, we assume that the vibronic SOC [33] between the S_1 and T_2 states is a process responsible for ISC in complex **1**, and, consequently, for the minor microsecond-scale emission in the visible region. This process is much less favourable with respect to the S_1-S_0 radiation relaxation, thus resulting in the fluorescence as the major pathway. A portion of absorbed energy could release as a phosphorescence from the T_1 state, but our calculations predict its manifestation in the infrared region. Thus, it is not detectable under the measurement conditions.

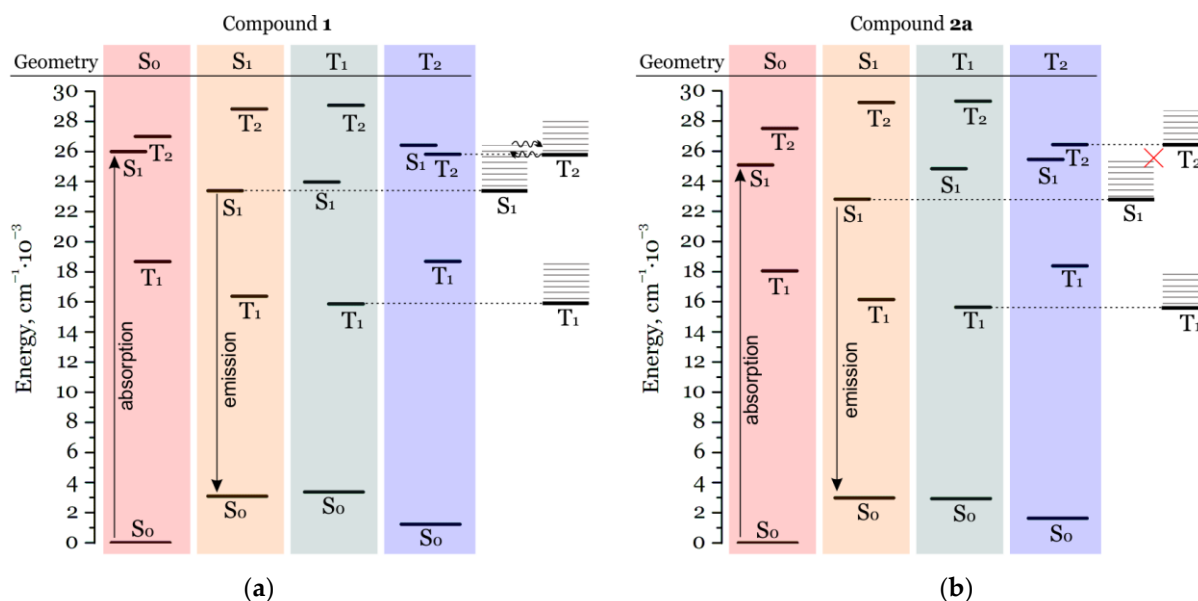


Figure 6. Representation of energy levels for different geometry states (S_0 , S_1 , T_1 , and T_2) of compounds **1** (a) and **2a,b** regarding the example of **2a** (b) in the energy range from 0 to $30 \times 10^3 \text{ cm}^{-1}$.

Complexes **2a** and **2b** exhibit a larger $\Delta E(S_1 - T_2)$ compared to complex **1**, and the vibrational sublevels for the S_1 and T_2 manifolds show almost null overlap. In addition, the potential energy surfaces for S_1 and T_2 do not intersect. This may be the reason why **2a** and **2b** do not show an afterglow signal. Figure 6 represents energy diagrams that summarize the different behaviours arising from the differences in the excited states of complexes **1** and **2a**. For **2b**, (Figure S13) the diagram is similar to that for **2a**.

3. Materials and Methods

3.1. General

All manipulations for the syntheses were performed using the Schlenk technique and a glovebox. Solvents were purified using the standard technique and stored under an argon atmosphere. The 1,3-aminophosphine was synthesized as described recently [28]. Elemental analyses were performed on various MICRO cube instruments (Langensfeld, Germany) for C, H, N, and S elements. IR-spectra were recorded on a Fourier IR spectrometer FT-801 (Simex, Novosibirsk, Russia) in KBr pellets. ^1H NMR spectra (500.13 MHz) and ^{31}P NMR spectra (202.45 MHz) were obtained with a Bruker DRX-500 spectrometer (Madison, Wisconsin, USA) in dry CDCl_3 at room temperature (RT); the solvent peak was used as an internal reference.

The diffuse reflectance UV-Vis spectra of the solid samples (Figure S14) were obtained with a Shimadzu UV-3101 spectrophotometer (Kyoto, Japan) at RT. Samples for the measurements were prepared by a thorough grinding of a mixture of the compounds under study (about 0.01 mol fraction) with BaSO_4 , which was also used as a standard. Spectral dependences of the diffuse reflectance were converted into spectra of a Kubelka-Munk function. Emission and excitation spectra of solids were recorded at RT on a Fluorolog 3 spectrometer (Horiba Jobin Yvon, Edison, NJ, USA) equipped with a cooled PC177CE-010 photon detection module (Horiba Jobin Yvon, Edison, NJ, USA) with a PMT R2658 photomultiplier (Horiba Jobin Yvon, Edison, NJ, USA). Excitation and emission spectra were corrected for source intensity (lamp and grating) and emission spectral response (detector and grating) by standard correction curves. For the measurements, powdered samples were placed between two nonfluorescent quartz plates. The emission decay curves were recorded on the same instrument using the TCSPC (time-correlated single photon counting) technique. A Horiba Nanoled laser diode (350 nm) was used as an excitation source. The curves were fitted by either one or two exponential decays; the fit yielded the emission

lifetime values. Absolute PL quantum yields (QY) for the solids were recorded using the Quanta- ϕ device of Fluorolog 3. For the photostability experiment, solid sample **1** was constantly irradiated under Ar conditions with a full-range spectrum Xe lamp ushio ux1450s-0 (450 W; Horiba Jobin Yvon, Edison, NJ, USA) for 1 h.

The UV-Vis spectra of the solutions in 1 cm quartz cuvettes in an argon atmosphere were obtained with Agilent Cary 60 spectrometer (Santa Clara, California, USA). The emission and excitation spectra of the same solutions were recorded on an Agilent Cary Eclipse spectrometer.

3.2. Theoretical Calculations

The ground state geometries were optimized in a vacuum, without any constraints, at the DFT level using the PBE0 functional [34], def2-TZVP(-f) basis set, def2-ECP effective core potential (60 core electrons) for the Au atoms and D3(BJ) dispersion correction. The equilibrium geometries of the S_1 (for **2a**) and T_2 states (for comparison between the geometries, see Figure S15) were optimized by TD(TDA)-PBE0-D3BJ/def2-TZVP(-f), and the T_1 state was optimized by UPBE0-D3BJ/def2-TZVP(-f) in the gaseous state, without any constraints. The equilibrium geometry of the S_1 state for **2b** was optimized by TD-BHandHLYP-D3BJ rather than TD-PBE0-D3BJ, because the optimization with the PBE0 functional yielded a twisted structure (Figure S16), with an underestimated energy of fluorescence. Optimization at the TD-BHandHLYP-D3BJ/def2-TZVP(-f) level of theory provided more reliable geometry and emission energy. The Frank-Condon and emission energies for all complexes were then calculated at the TD(A)-PBE0/def2-TZVP(-f) level. Regular TD-DFT was used for the singlet states, and the Tamm-Dancoff approximation of TD-DFT was used for the triplet states due to triplet instability problems in TD-DFT [35]. For the acceleration of calculations resolution of identity for the Coulomb part (RI) and the chain of spheres for the Fock exchange (COSX), approximations were used with the corresponding auxiliary basis [36,37]. Correspondence to the minima of optimized geometries were verified by analytical harmonic vibrational frequency calculations for the ground states and T_1 (UKS), and by numerical harmonic vibrational frequency calculations for the excited states.

The scalar-relativistic ZORA method was used with the SARC-ZORA-TZVP basis set for Au atoms to take into account relativistic effects in the photophysical properties; the ZORA-def2-TZVP basis set was used for the other atoms with SARC/J and AutoAux auxiliary basis sets for acceleration via the RIJCOSX algorithm. The quasi-degenerate perturbation theory was used for the calculation of spin-orbital coupling regarding the ZORA-TDA-DFT results [38]. The SOC integrals were calculated by the RI-SOMF(1X) method [39]. The calculations of SOC between states do not include vibronic coupling and non-adiabatic couplings. All geometry optimizations and TD(TDA)-DFT calculations were conducted using the Orca 4.2.1 program. Molecular orbitals were visualized using ChemCraft 1.8.

Vibronically resolved fluorescence (from S_1 state) and phosphorescence (from T_1 and T_2 states) spectra were calculated by the path integral approach implemented in the ESD subprogram of Orca 5.0.3. Low-energy normal modes were cut due to their anharmonicity (TCutFreq value is 100 cm^{-1}). The line shape was set by VOIGT option, which is the mean product of the Gaussian and Lorentzian curves (Linew parameter is 20 cm^{-1} and Inlinew parameter is 100 cm^{-1}).

3.3. Syntheses

3.3.1. Synthesis of PN

At $0\text{ }^\circ\text{C}$, a solution of Ph_2PCI (0.594 mL, 3.31 mmol) in toluene (5 mL) was added dropwise to a solution of $\text{NH}_2\text{-btd}$ (0.500 g, 3.31 mmol) and Et_3N (0.922 mL, 6.62 mmol) in toluene (5 mL). The resulting mixture was allowed to warm up to RT and stirred overnight. The precipitate of $\text{Et}_3\text{N}\cdot\text{HCl}$ was removed by filtration and rinsed four times with 3 mL of toluene. The solutions were combined, and all volatiles were evaporated. The residue

was purified by column chromatography (silica gel, ethyl acetate:hexane = 1:10), followed by recrystallization from diethyl ether. Yield 0.876 g (79%). Calc. for $C_{18}H_{14}N_3PS$ (335.36): C 64.5, H 4.2, N 12.5, S 9.6. Found C 64.4, H 4.4, N 12.1, S 9.8. $^{31}P\{H\}$ NMR (C_6D_6 , δ , ppm): 28.4 (s). 1H NMR (C_6D_6 , δ , ppm): 7.45–7.42 (m, 4H), 7.19–7.03 (m, 5H, 1H from btd-H + solvent), 7.06–7.03 (m, 7H), 5.96 (d, 1H). IR-spectrum (KBr, cm^{-1}): 3281 s, 3050 m, 3000 w, 1599 w, 1541 s, 1487 s, 1433 s, 1383 s, 1290 m, 1082 s, 1044 m, 1024 w, 905 s, 850 m, 816 m, 739 s, 696 s.

3.3.2. Synthesis of $[Au(PN)Cl]$ (**1**)

A mixture of *PN* (25 mg, 0.0745 mmol) and (THT)AuCl (24 mg, 0.0745 mmol) was dissolved in CH_3CN and was stirred at RT overnight to give a clear solution. The solvent was evaporated, and the oil residue was extracted by toluene in vacuum at 60 °C to obtain a yellow crystalline product. Yield: 25 mg (74%). Calc. for $C_{18}H_{14}AuClN_3PS$ (567.78 g/mol): C 38.1, H 2.5, N 7.4, S 5.6. Found C 37.8, H 2.4, N 7.0, S 6.1. $^{31}P\{H\}$ NMR ($CDCl_3$, δ , ppm): 57.46 (s). 1H NMR ($CDCl_3$, δ , ppm): 7.88–7.83 (m, 4H), 7.67–7.63 (m, 2H), 7.60–7.57 (m, 5H), 7.45 (dd, 1H, $J_1 = 9$ Hz, 7.4 Hz), 7.13 (d, 1H, $J = 7.3$ Hz), 6.01 (d, 1H, $J = 4.7$ Hz). IR (cm^{-1}): 3372 (m), 3045 (w), 2919 (w), 2850 (w), 2016 (w), 1993 (w), 1962 (w), 1940 (w), 1917 (w), 1890 (w), 1816 (w), 1728 (w), 1696 (w), 1642 (w), 1607 (w), 1545 (s), 1489 (m), 1436 (m), 1379 (s), 1298 (m), 1270 (w), 1180 (w), 1160 (w), 1109 (s), 1084 (s), 1043 (w), 1001 (w), 909 (s), 872 (m), 828 (w), 797 (w), 763 (w), 743 (s), 717 (w), 707 (w), 690 (s), 655 (w).

3.3.3. Synthesis of $[Au(PCN)Cl]$ (**2a**)

A mixture of *PCN* (50 mg, 0.118 mmol) and (THT)AuCl (38 mg, 0.118 mmol) was dissolved in THF (5 mL). The yellowish solution was stirred at RT overnight and concentrated under vacuum. A portion of crystals suitable for single-crystal XRD analysis was formed after exposure of the solution at 2 °C for 1 day. The crystals were separated and washed with diethyl ether. The mother liquor was further concentrated to isolate an additional portion of the compound. The fine powder was separated and washed with diethyl ether. Total yield: 75 mg (97%). Calc. for $AuC_{25}H_{20}N_3PSCl$ (657.90 g/mol): C 45.6, H 3.1, N 6.4, S 4.9. Found C 46.1, H 3.2, N 6.2, S 5.1. $^{31}P\{H\}$ NMR ($CDCl_3$, δ , ppm): 44.4 (s). 1H NMR ($CDCl_3$, δ , ppm): 7.76 (dd, 2H), 7.52 (t, 1H), 7.46–7.38 (m, 5H), 7.30 (t, 2H), 7.25 (d, 2H), 7.20–7.12 (m, 5H), 6.31 (p, 1H), 6.03 (t, 1H), 5.68 (dd, 1H). IR (cm^{-1}): 3353 (m), 3056 (m), 2912 (m), 2853 (w), 1971 (w), 1901 (w), 1804 (w), 1606 (w), 1550 (s), 1494 (s), 1434 (s), 1408 (s), 1364 (w), 1298 (s), 1183 (m), 1124 (w), 1105 (s), 1079 (w), 1026 (w), 1000 (w), 916 (w), 900 (m), 853 (m), 830 (m), 796 (m), 777 (w), 735 (s), 694 (s), 632 (w).

3.3.4. Synthesis of $[Au(PCN)Cl]$ (**2b**)

The compound is obtained by fast concentration of a solution of **2** in THF to give an oily sample. Subsequent exposure of the sample in a small amount of THF yielded a portion of crystals **2b**. To obtain bulk **2b**, a portion of the obtained crystals was sown on an oversaturated solution of the compound in THF. Calcd for $AuC_{25}H_{20}N_3PSCl$ (657.90 g/mol): C 45.6, H 3.1, N 6.4, S 4.9; found C 45.9, H 3.1, N 6.3, S 4.8. IR (cm^{-1}): 3396 (m), 3067 (w), 3023 (w), 2903 (w), 1606 (w), 1552 (s), 1500 (s), 1436 (w), 1413 (m), 1368 (w), 1308 (m), 1198 (w), 1130 (w), 1104 (m), 1077 (w), 1030 (w), 1000 (w), 901 (m), 855 (w), 832 (w), 797 (w), 776 (w), 740 (s), 695 (s), 557 (m).

3.4. X-ray Data

Single-crystal XRD data for compounds **1–2** (Tables S9–S11) were collected at 150 K with a Bruker D8 Venture diffractometer (Madison, Wisconsin, USA) with a CMOS PHOTON III detector (Bruker, Madison, Wisconsin, USA) and $I\mu S$ 3.0 microfocus source (MoK α radiation ($\lambda = 0.71073$ Å), collimating Montel mirrors; Incoatec GmbH, Geesthacht, Germany). The crystal structures were solved using the SHELXT [40] and were refined using the SHELXL [41] programs with OLEX2 GUI [42]. Atomic displacement parameters for non-

hydrogen atoms were refined anisotropically. Hydrogen atoms were placed geometrically, with the exception of those in the amino groups, which were localized from the residual electron density map and refined with the restraining of the N–H bond (0.88 Å). The structures of **1–2** were deposited to the Cambridge Crystallographic Data Centre (CCDC) as a supplementary publication, No. 2217671–2217673.

Powder XRD data for the compounds (Figures S1–S3) were collected at RT with a Bruker D8 Advance diffractometer in Bragg–Brentano geometry with an energy discriminating Eyger XE T detector (CuK α radiation).

4. Conclusions

In summary, we synthesized Au(I) compounds **1–2** comprising closely related *PN* and *PCN* ligands. The latter comprise NH-btd moiety as a chromophore, and PPh₂ moiety as a readily accessible unit for the metal coordination. The main difference between the ligands is that one of them (*PN*) contains a P–N bond, while in the other (*PCN*), the P and N atoms are separated by a methylene bridge (Scheme 1). Such differences alter the nature of the luminescence of the corresponding complexes: polymorphs **2a** and **2b** exclusively exhibit fluorescence, which is not typical of Au(I) compounds, while compound **1** reveals fluorescence as the major radiative pathway, and a minor contribution of the microsecond-scale component.

We interpreted the unusual fluorescent behaviour using quantum chemical TD(A)-DFT calculations. In the complexes, the frontier molecular orbitals, responsible for the S₀–S₁ and S₀–T₁ transitions, are located almost exclusively on the *PN* and *PCN* ligands, i.e., the transitions mainly have an intraligand nature. Owing to the overall small metal contribution to the orbitals, the SOC is small. In addition, the T₁ state has much lower energy than does the S₁ (by ca. 7000 cm^{−1}) state, which further hinders the ISC from S₁. It thus enables the latter state to decay in the form of fluorescence as a dominant radiative process. In the specific case of complex **1**, the emission origin is not only limited to the prompt S₁ decay, but also occurs with a mixing of singlet and triplet states, resulting in the presence of a minor microsecond-scale component. This behaviour is probably governed by a small contribution of (M+X)LCT, in the case of **1**, which is absent in **2a** and **2b**. As a possible channel, the SOC between the S₁ and T₂ states can contribute to ISC, owing to rich vibronic structure of the corresponding singlet and triplet manifolds.

Supplementary Materials: The following supporting information can be downloaded at: <https://www.mdpi.com/article/10.3390/molecules27238162/s1>, Figures S1–S3: Simulated and experimental powder XRD patterns; Tables S1–S6: DFT calculation of Frank–Condon excitation processes; Figures S4 and S5: Frontier molecular orbitals of **1–2** in their S₀ optimized geometry; Figure S6: UV-Vis, emission and excitation spectra of the solids; Figure S7: UV-Vis, emission, and excitation spectra of **2** in THF; Figures S8–S10: Emission decay kinetics for the compounds; Figure S11: Emission of the compounds at 77–300 K; Tables S7 and S8: Calculated values of selected spin-orbit coupling matrix elements for the complexes; Figure S12: Comparison of frontier orbitals of complex **1** in different equilibrium geometries; Figure S13: Representation of energy levels for different geometry states of the complexes; Figure S14: IR-spectra of the compounds; Figure S15: Comparison of equilibrium geometries of the complexes in different states; Figure S16: Overlaid geometries for S₁ equilibrium state of **2b** obtained by two different DFT methods. Table S9: Crystal data and structure refinement for the compounds; Table S10: Selected bond lengths for the structures; Table S11: Selected bond angles for the structures.

Author Contributions: Conceptualization, T.S.S.; funding acquisition, T.S.S.; investigation, R.M.K., A.A.R. and T.S.S.; supervision, S.N.K.; visualization, R.M.K. and T.S.S.; writing—original draft, R.M.K.; writing—review and editing, S.N.K. and T.S.S. All authors have read and agreed to the published version of the manuscript.

Funding: This research was funded by the Russian Science Foundation (project no. 21-73-10096). Powder XRD and luminescence kinetics studies were supported by the Ministry of Science and Higher Education of the Russian Federation (No. 121031700313-8 and No. 121031700321-3).

Institutional Review Board Statement: Not applicable.

Informed Consent Statement: Not applicable.

Data Availability Statement: Not applicable.

Acknowledgments: We are grateful to the Irkutsk Supercomputer Center of SB RAS for providing access to the HPC-cluster «Akademik V.M. Matrosov» (Irkutsk Supercomputer Center of SB RAS, Irkutsk: ISDCT SB RAS; <http://hpc.icc.ru>, accessed on 3 November 2022).

Conflicts of Interest: The authors declare no conflict of interest.

Sample Availability: Samples of compounds 1–2 are available from the authors.

References

1. Tao, Y.; Wang, Y.; Hu, S.; Young, D.J.; Lu, C.; Li, H.-X.; Ren, Z.-G. A photoluminescent Au(I)/Ag(I)/PNN coordination complex for relatively rapid and reversible alcohol sensing. *Dalton Trans.* **2021**, *50*, 6773–6777. [[CrossRef](#)]
2. He, X.; Yam, V.W.-W. Luminescent gold(I) complexes for chemosensing. *Coord. Chem. Rev.* **2011**, *255*, 2111–2123. [[CrossRef](#)]
3. Cheng, S.; Chen, Z.; Yin, Y.; Sun, Y.; Liu, S. Progress in mechanochromic luminescence of gold(I) complexes. *Chin. Chem. Lett.* **2021**, *32*, 3718–3732. [[CrossRef](#)]
4. Kinzhalov, M.A.; Grachova, E.V.; Luzyanin, K.V. Tuning the luminescence of transition metal complexes with acyclic diaminocarbenes ligands. *Inorg. Chem. Front.* **2022**, *9*, 417–439. [[CrossRef](#)]
5. Jin, M.; Ito, H. Solid-state luminescence of Au(I) complexes with external stimuli-responsive properties. *J. Photochem. Photobiol. C* **2022**, *51*, 100478. [[CrossRef](#)]
6. Shafikov, M.Z.; Daniels, R.; Kozhevnikov, V.N. Unusually fast phosphorescence from Ir(III) complexes via dinuclear molecular design. *J. Phys. Chem. Lett.* **2019**, *10*, 7015–7024. [[CrossRef](#)]
7. Petrovskii, S.K.; Paderina, A.V.; Sizova, A.A.; Baranov, A.Y.; Artem'ev, A.A.; Sizov, V.V.; Grachova, E.V. Luminescence behaviour of Au(I)–Cu(I) heterobimetallic coordination polymers based on alkynyl-tris(2-pyridyl)phosphine Au(I) complexes. *Dalton Trans.* **2020**, *49*, 13430–13439. [[CrossRef](#)] [[PubMed](#)]
8. Au-Yeung, C.C.; Li, L.-K.; Tang, M.-C.; Lai, S.-L.; Cheung, W.-L.; Ng, M.; Chan, M.-Y.; Yam, V.W.-W. Molecular design of efficient yellow- to red-emissive alkynylgold(III) complexes for the realization of thermally activated delayed fluorescence (TADF) and their applications in solution-processed organic light-emitting devices. *Chem. Sci.* **2021**, *12*, 9516–9527. [[CrossRef](#)]
9. Baranov, A.Y.; Slavova, S.O.; Berezin, A.S.; Petrovskii, S.K.; Samsonenko, D.G.; Bagryanskaya, I.Y.; Fedin, V.P.; Grachova, E.V.; Artem'ev, A.V. Controllable synthesis and luminescence behavior of tetrahedral Au@Cu₄ and Au@Ag₄ clusters supported by tris(2-pyridyl)phosphine. *Inorg. Chem.* **2022**, *61*, 10925–10933. [[CrossRef](#)]
10. Shakirova, J.R.; Grachova, E.V.; Gurzhiy, V.V.; Koshevoy, I.O.; Melnikov, A.S.; Sizova, O.V.; Tunik, S.P.; Laguna, A. Luminescent heterometallic gold–copper alkynyl complexes stabilized by tridentate phosphine. *Dalton Trans.* **2012**, *41*, 2941–2949. [[CrossRef](#)]
11. Feuerstein, W.; Holzer, C.; Gui, X.; Neumeier, L.; Klopfer, W.; Breher, F. Synthesis of new donor-substituted biphenyls: Pre-ligands for highly luminescent (C[∞]C[∞]D) gold(III) pincer complexes. *Chem. Eur. J.* **2020**, *26*, 17156–17164. [[CrossRef](#)]
12. Moitra, T.; Karak, P.; Chakraborty, S.; Ruud, K.; Chakrabarti, S. Behind the scenes of spin-forbidden decay pathways in transition metal complexes. *Phys. Chem. Chem. Phys.* **2021**, *23*, 59–81. [[CrossRef](#)]
13. Artem'ev, A.V.; Demyanov, Y.V.; Rakhmanova, M.I.; Bagryanskaya, I.Y. Pyridylarsine-based Cu(I) complexes showing TADF mixed with fast phosphorescence: A speeding-up emission rate using arsine ligands. *Dalton Trans.* **2022**, *51*, 1048–1055. [[CrossRef](#)]
14. Demyanov, Y.V.; Sadykov, E.H.; Rakhmanova, M.I.; Novikov, A.S.; Bagryanskaya, I.Y.; Artem'ev, A.V. Tris(2-pyridyl)arsine as a new platform for design of luminescent Cu(I) and Ag(I) complexes. *Molecules* **2022**, *27*, 6059. [[CrossRef](#)]
15. Mořka, M.; Serdiuk, I.E.; Kozakiewicz, K.; Hoffman, E.; Szumilas, J.; Kubicki, A.; Park, S.Y.; Bojarski, P. Understanding the internal heavy-atom effect on thermally activated delayed fluorescence: Application of Arrhenius and Marcus theories for spin–orbit coupling analysis. *J. Mater. Chem. C* **2022**, *10*, 7925–7934. [[CrossRef](#)]
16. Tong, G.S.M.; Chow, P.K.; Che, C.-M. Where is the heavy-atom effect? Role of the central ligand in tetragold(I) ethynyl complexes. *Angew. Chem. Int. Ed.* **2010**, *49*, 9206–9209. [[CrossRef](#)]
17. Mihaly, J.J.; Stewart, D.J.; Grusenmeyer, T.A.; Phillips, A.T.; Haley, J.E.; Zeller, M.; Gray, T.G. Photophysical properties of organogold(I) complexes bearing a benzothiazole-2,7-fluorenyl moiety: Selection of ancillary ligand influences white light emission. *Dalton Trans.* **2019**, *48*, 15917–15927. [[CrossRef](#)]
18. Abramova, E.O.; Paderina, A.V.; Slavova, S.O.; Kostenko, E.A.; Eliseenkov, E.V.; Petrovskii, S.K.; Gitlina, A.Y.; Boyarskiy, V.P.; Grachova, E.V. Just add the gold: Aggregation-induced-emission properties of alkynylphosphinegold(I) complexes functionalized with phenylene–terpyridine subunits. *Inorg. Chem.* **2021**, *60*, 18715–18725. [[CrossRef](#)] [[PubMed](#)]
19. Deng, D.; Suo, B.; Zou, W. New Light on an Old Story: Breaking Kasha's rule in phosphorescence mechanism of organic boron compounds and molecule design. *Int. J. Mol. Sci.* **2022**, *23*, 876. [[CrossRef](#)]
20. Shekhovtsov, N.A.; Kokina, T.E.; Vinogradova, K.A.; Panarin, A.Y.; Rakhmanova, M.I.; Naumov, D.Y.; Pervukhina, N.V.; Nikolaenkova, E.B.; Krivopalov, V.P.; Czerwieńiec, R.; et al. Near-infrared emitting copper(I) complexes with a pyrazolylpyrimidine ligand: Exploring relaxation pathways. *Dalton Trans.* **2022**, *51*, 2898–2911. [[CrossRef](#)]

21. Chan, K.T.; Tong, G.S.M.; To, W.-P.; Yang, C.; Du, L.; Phillips, D.L.; Che, C.-M. The interplay between fluorescence and phosphorescence with luminescent gold(I) and gold(III) complexes bearing heterocyclic arylacetylide ligands. *Chem. Sci.* **2017**, *8*, 2352–2364. [[CrossRef](#)] [[PubMed](#)]
22. Moitra, T.; Alam, M.M.; Chakrabarti, S. Intersystem crossing rate dependent dual emission and phosphorescence from cyclometalated platinum complexes: A second order cumulant expansion based approach. *Phys. Chem. Chem. Phys.* **2018**, *20*, 23244–23251. [[CrossRef](#)] [[PubMed](#)]
23. Pinto, A.; Echeverri, M.; Gómez-Lor, B.; Rodríguez, L. How to achieve near unity fluorescence quantum yields on gold(I) benzothiadiazole-based derivatives. *Dyes Pigm.* **2022**, *202*, 110308. [[CrossRef](#)]
24. Sukhikh, T.S.; Ogienko, D.S.; Bashirov, D.A.; Konchenko, S.N. Luminescent complexes of 2,1,3-benzothiadiazole derivatives. *Russ. Chem. Bull.* **2019**, *68*, 651–661. [[CrossRef](#)]
25. Sukhikh, T.S.; Khisamov, R.M.; Bashirov, D.A.; Komarov, V.Y.; Molokeev, M.S.; Ryadun, A.A.; Benassi, E.; Konchenko, S.N. Tuning of the coordination and emission properties of 4-amino-2,1,3-benzothiadiazole by introduction of diphenylphosphine group. *Cryst. Growth Des.* **2020**, *20*, 5796–5807. [[CrossRef](#)]
26. Pylova, E.K.; Khisamov, R.M.; Bashirov, D.A.; Sukhikh, T.S.; Konchenko, S.N. The effect of halides and coordination mode of 4-amino-2,1,3-benzothiadiazole on the luminescence properties of its Zn complexes. *CrystEngComm* **2022**, *accepted manuscript*. [[CrossRef](#)]
27. Ceriani, C.; Corsini, F.; Mattioli, G.; Mattiello, S.; Testa, D.; Po, R.; Botta, C.; Griffini, G.; Beverina, L. Sustainable by design, large Stokes shift benzothiadiazole derivatives for efficient luminescent solar concentrators. *J. Mater. Chem. C* **2021**, *9*, 14815–14826. [[CrossRef](#)]
28. Khisamov, R.M.; Ryadun, A.A.; Konchenko, S.N.; Sukhikh, T.S. Molecular environment effects that modulate the photophysical properties of novel 1,3-phosphinoamines based on 2,1,3-benzothiadiazole. *Molecules* **2022**, *27*, 3857. [[CrossRef](#)]
29. Patrizi, B.; Iagatti, A.; Abbondanza, L.; Bussotti, L.; Zanardi, S.; Salvalaggio, M.; Fusco, R.; Foggi, P. Ultrafast intramolecular and solvation dynamics in 4,7-bis(4,5-dibutylbenzo[1,2-b:4,3-b']bisthiophene[1,2-b:4,3-b']bisthiophen-2-yl)-2,1,3-benzothiadiazole. *J. Phys. Chem. C* **2019**, *123*, 5840–5852. [[CrossRef](#)]
30. Pritchina, E.A.; Gritsan, N.P.; Rakitin, O.A.; Zibarev, A.V. 2,1,3-Benzochalcogenadiazoles: Regularities and peculiarities over a whole chalcogen pentad O, S, Se, Te and Po. *Targets Heterocycl. Syst.* **2019**, *23*, 143–154. [[CrossRef](#)]
31. Plyuta, N.; Cauchy, T.; Hauser, A.; Lloret, F.; Julve, M.; Avarvari, N. Zinc(II) and copper(II) complexes with benzothiadiazole Schiff-base ligands. *Polyhedron* **2022**, *224*, 115994. [[CrossRef](#)]
32. Shafikov, M.Z.; Kozhevnikov, D.N.; Bodensteiner, M.; Brandl, F.; Czerwieniec, R. Modulation of intersystem crossing rate by minor ligand modifications in cyclometalated platinum(II) complexes. *Inorg. Chem.* **2016**, *55*, 7457–7466. [[CrossRef](#)] [[PubMed](#)]
33. Rodriguez-Serrano, A.; Rai-Constapel, V.; Daza, M.C.; Doerr, M.; Marian, C.M. Internal heavy atom effects in phenothiazinium dyes: Enhancement of intersystem crossing via vibronic spin–orbit coupling. *Phys. Chem. Chem. Phys.* **2015**, *17*, 11350–11358. [[CrossRef](#)] [[PubMed](#)]
34. Perdew, J.P.; Burke, K.; Ernzerhof, M. Generalized gradient approximation made simple. *Phys. Rev. Lett.* **1996**, *77*, 3865–3868. [[CrossRef](#)]
35. Peach, M.J.G.; Tozer, D.J. Overcoming low orbital overlap and triplet instability problems in TDDFT. *J. Phys. Chem. A* **2012**, *116*, 9783–9789. [[CrossRef](#)]
36. Izsák, R.; Neese, F. An overlap fitted chain of spheres exchange method. *J. Chem. Phys.* **2011**, *135*, 144105. [[CrossRef](#)]
37. Izsák, R.; Neese, F.; Klopper, W. Robust fitting techniques in the chain of spheres approximation to the Fock exchange: The role of the complementary space. *J. Chem. Phys.* **2013**, *139*, 094111. [[CrossRef](#)]
38. de Souza, B.; Neese, F.; Izsák, R. On the theoretical prediction of fluorescence rates from first principles using the path integral approach. *J. Chem. Phys.* **2018**, *148*, 034104. [[CrossRef](#)]
39. Neese, F. Efficient and accurate approximations to the molecular spin-orbit coupling operator and their use in molecular g-tensor calculations. *J. Chem. Phys.* **2005**, *122*, 034107. [[CrossRef](#)]
40. Sheldrick, G.M. SHELXT—Integrated space-group and crystal-structure determination. *Acta Crystallogr. Sect. A* **2015**, *71*, 3–8. [[CrossRef](#)]
41. Sheldrick, G.M. Crystal structure refinement with SHELXL. *Acta Crystallogr. Sect. C* **2015**, *71*, 3–8. [[CrossRef](#)] [[PubMed](#)]
42. Dolomanov, O.V.; Bourhis, L.J.; Gildea, R.J.; Howard, J.A.K.; Puschmann, H. OLEX2: A complete structure solution, refinement and analysis program. *J. Appl. Crystallogr.* **2009**, *42*, 339–341. [[CrossRef](#)]